Development of small-scale experiments for the education of chemical engineering and its practice for undergraduates

Kenji Katayama[1,2*], Risa Ichinose[1] Yuki Konno[1], Woon Yong Sohn,[1] Shota Kuwahara,[3] Toshitaka Funazukuri[1]

1 Department of Applied Chemistry, Chuo University, Tokyo 112-8551, Japan

2 PRESTO, Japan Science and Technology Agency (JST), Saitama 332-0012, Japan

3 Department of Chemistry, Toho University, 2-2-1 Miyama, Funabashi, Chiba 274-8510, Japan

*Corresponding authors:

K. Katayama, Phone: +81-3-3817-1913, E-mail: kkata@kc.chuo-u.ac.jp

Abstract

A series of small-scale/micro-scale experiments used for the education of undergraduate students in chemical engineering courses have been developed. Based on the “small-scale/micro-scale” concept, the experiments were developed to provide an intuitive understanding of chemical processes, both by increasing the visibility of these chemical processes and by making the apparatus compact (desktop size). Nine experiments were developed that are relevant to the fields of thermal engineering, fluid engineering, unit operations, and reaction engineering. These experiments were introduced during the educational experiment course for undergraduates in the chemical engineering program.

Keywords: small-scale experiment, chemical engineering

Introduction

Small-scale/micro-scale experiments represent a concept for “green” education that utilizes a small device and a small amount of chemicals. Small-scale experiments are not only small and good for the environment, but they are also effective in terms of education. This is because they create an intuitive understanding of chemical processes due to the visibility and compactness of small-scale experiments, enabling individual experiments and representing a promising concept for the education of chemistry students at any level.

The concept of “small-scale/micro-scale” experiments was proposed since the 1940s,(Wright and Eastcott, 1949; Stock, 1953; Horak and Crist, 1975) However, in the 1990s this concept rapidly expanded, and various reactions and chemistry equipment for small-scale/micro-scale experiments were developed (Kelkar and Dhavale, 2000) Additionally, various techniques were collected in the microscale laboratory in the Journal of Chemical Education (Zipp, 1989) and a book was published by the Royal Society of Chemistry (Skinner, 1997). At an early stage, the experiments were intended for middle/high school students (Grønneberg *et al.*, 2006; Supasorn, 2015) A variety of experiments and demonstrations has been developed to promote science awareness (Néel *et al.*, 2015; Chien *et al.*, 2018) and demonstration (Lee and Wiener, 2011). After a while, the experiments were extended to higher levels of education (Flash, 1990) and various chemical processes were changed into small-scale procedures such as distillation (Schwartz, 1992) and the extraction of products (McKenzie *et al.*, 2004). In particular, this concept aligns with the field of organic chemistry (Wright and Eastcott, 1949; Stock, 1990; Gilow, 1991; Sobral, 2005) and several books summarizing the methods have been published (Pavia *et al.*, 2007). A series of experiments was summarized in books about general chemistry (Szafran *et al.*, 1993; Skinner, 1997) and inorganic chemistry (Szafran *et al.*, 1991), as well. Some of the analytical equipment was prepared with small-scale devices such as gas chromatography (Vrtacnik and Gros, 2005) and electrophoreses.(Brooks and Brooks, 1995) Various small-scale experiments for thermodynamics have also been developed (Brouwer, 1991), and now several companies have commercialized the small experimental devices combined with sensor equipment. Some unique experiments have also been developed; for example, the color change study involving solvatochromism in biofuels has recently been introduced for undergraduate study (El Seoud *et al.*, 2011). The interaction between proteins is studied by enzyme-linked immunosorbent assay (ELISA)(Johnson *et al.*, 2017). In recent years, the Lab-on-a-Chip type of fluidic device has been introduced for chemical education (Tabassum *et al.*, 2018; Wietsma *et al.*, 2018) and used for organic and inorganic syntheses (Feng *et al.*, 2015).

The study of chemical engineering, which is requisite for working in the chemical industry, is one of the key subjects in the engineering components of chemistry departments in universities, as it

supports companies by educating chemical engineers. In the course of their study of chemical engineering, students learn “mass transfer,” “heat transfer,” “unit operations,” “reaction engineering,” etc., which constitute the knowledge necessary to design and manufacture the infrastructure of chemical plants.

In terms of education in chemical engineering, learners face two main difficulties. One is that many empirical equations are given without sound reasoning for using them, which includes various non-dimensional numbers utilized for the common understanding of thermal, fluidic, and mass transport phenomena without performing all the experiments or calculations when the experimental scale changes. The other is that each chemical process is frequently invisible because the equipment is a black box or tends to be large like actual applications in the chemical industry. In student lab courses for chemical engineering, large equipment with complicated functions have frequently been utilized, which has made it difficult for learners to understand the actual processes. One of the solutions is to utilize computer-based learning to facilitate an understanding of the processes by assuming various chemical engineering models (Squires *et al.*, 1992; Selmer *et al.*, 2007).

We have developed small-scale/micro-scale experiments for undergraduates in the field of general chemistry and physical chemistry. In addition, we have come up with an idea: that the concept of small-scale/micro-scale experiments will help create an understanding of chemical engineering among undergraduates. By utilizing small devices instead of large black-box devices, learners can understand each chemical process intuitively. The simpler processes foster a better understanding of theoretical equations, which could lead to more complicated theories for further study.

In the last five years, we have developed ~10 small-scale/micro-scale experiments that provide education in chemical engineering in a chemistry department in Japan. They have been put into practice as a course for education in the chemical engineering field. This paper introduces the developed experiments and also describes their merits.

Concept

In each experiment, we aimed to achieve an intuitive understanding among learners by improving the visibility of experiments and making a compact desktop device. To help learners understand more clearly, we prepared simplified chemical processes for experiments, which can be further extended into complicated issues. A small amount of chemicals was used to reduce the cost of the experiments, as well as to make the learners aware of the environmental issues related to chemical experiments, similar to those of other small-scale concepts. In general, the cost of each experiment was less than $1,000 for each experiment per group (2-4 members expected), designed as they have been adopted by other universities.

We designed the series of experiments along with a curriculum for chemical engineering education,

which is categorized into thermal engineering, fluid engineering, unit operations, reaction engineering and other subjects such as particle engineering, process design, etc. Following are the titles of the experiments in each category.

Thermal engineering:

- Thermal conduction in metals
- Thermal convection for double pipe thermal exchanger

Fluid engineering

- Pressure loss in tubes and velocity measurements of fluids

Unit operations

- Distillation
- Gas adsorption on solid medium
- Gas absorption by liquid

Reaction engineering

- Reaction rate difference for various reactors
- High-pressure gas

Others

- Particle size measurement

Series of experiments

1. Thermal engineering

1.1 Thermal conduction in metals

Thermal management is one of the most important issues for controlling and optimizing the production efficiency of chemicals. In the thermal management of chemical processes, we must understand three types of heat transfer processes; thermal conduction, thermal convection, and radiative heat transfer. The first one represents the thermal conduction in a stationary material (Hatzikraniotis *et al.*, 2010). The second one represents the heat transfer in a fluidic material. The third one corresponds to electromagnetic energy transfer. In the study on heat transfer, it is difficult to understand the processes because of the invisibility of heat. To overcome this problem, we utilized thermography to understand thermal processes by visualizing them. In recent years, thermography has been utilized for education in various fields due to a reduction in its price (Möllmann and Vollmer, 2007; Haglund *et al.*, 2015).

In thermal conduction, the thermal energy transfer is expressed by Fourier's law:

$$Q = -kA\, dT/dx\ , \qquad (1.1)$$

where Q is the input of the thermal energy, k is the thermal conductivity, A is the cross sectional area, and dT/dx is the temperature gradient. Under the steady state, integrating from x = 0 to L, and T = T_1

to T_2,

$$Q = \frac{kA}{L}(T_1 - T_2)\,, \qquad (1.2)$$

The linear temperature profile is obtained when Q remains constant. On the other hand, under the unsteady state, the temperature profile in the one-dimensional case is given by the thermal diffusion equation as:

$$\frac{\partial T}{\partial t} = D\left(\frac{\partial^2 T}{\partial x^2}\right),\ D = \frac{k}{\rho C_P}\,, \qquad (1.3)$$

where D is the thermal diffusion coefficient, ρ is the density, and C_P is the heat capacity.

In this experiment, the heat transfer of metal rods is measured using a thermography device. An end of the metal rod is heated with a temperature-controlled heater, and the temperature profile in the rod is visualized. A thermography device can observe not only the static condition of temperature but also the unsteady state thermal conduction. The experimental apparatus is shown in Figure.1. Another metal rod surrounded by a temperature-controlled rubber heater was used as a heater, which had silicone paste on the edge to maintain good thermal contact. The temperature profile was measured after the heater metal had been put in contact with a sample metal rod by a hand-held thermography device (FLIR E5) attached to a stage. We prepared rods made of copper, iron, brass, aluminum, and stainless steel with the same size of 10x1x0.5 cm.

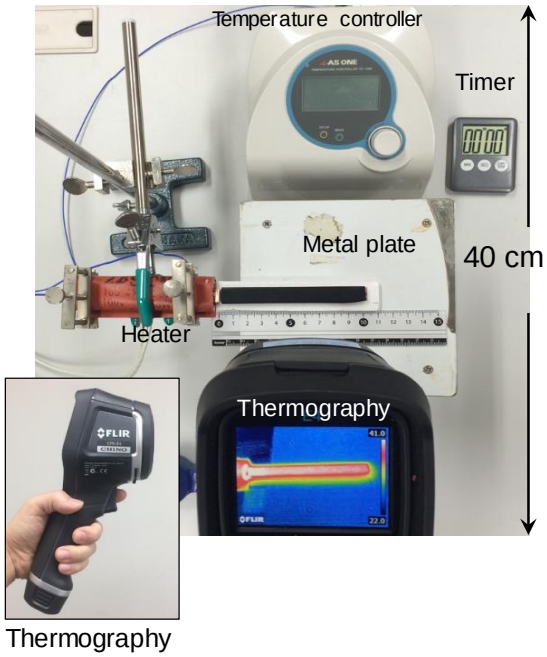

Fig. 1 The apparatus of thermal conduction experiment. A rubber heater was put into contact with a metal rod from the side, and the temperature of the heater was controlled. The temperature profile was measured using a hand-held thermography device.

142

143 The temperature profiles for copper and steel under the steady state are shown in Figure 2 (left).
144 The profiles were measured for over 300 seconds after the heater metal came into contact with a
145 sample metal rod. It is obvious that the heat reached a more distant position for copper than it did for
146 steel, which can be studied using Fourier's law under the steady state; thus, learners can understand
147 the difference between the thermal conductivities of different materials. Furthermore, a thermography
148 measurement provides a real-time temperature profile of an object, while the thermal conduction under
149 the unsteady state can also be studied. Figure 2 (right) shows the time evolution of the temperature
150 profile for a rod of steel. It is recognized that the heat was transferred from the heater side to the other
151 end. Because it is designed in one-dimensional thermal conduction by using a rod structure, the result
152 can be compared with a simple calculation obtained from the one-dimensional thermal conduction.
153 The unsteady state thermal conduction was calculated by an Excel chart via numerical calculation, and
154 the result was compared to create an understanding of how the theory could explain the heat transfer.
155 The visualization of the temperature profile in real-time for a variety of materials helps create an
156 intuitive understanding of the thermal conduction processes under steady and unsteady states.

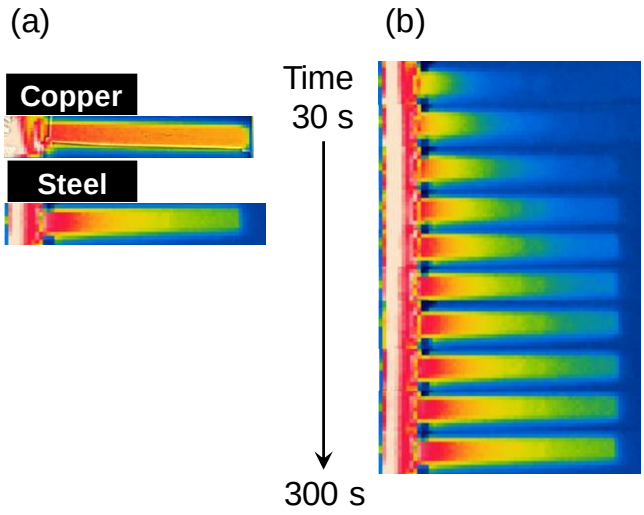

Fig. 2 (a) The temperature profiles after thermal equilibrium was reached for different metal rods; copper and steel. (b) The time sequence of the temperature change for a steel rod with an interval of 30 seconds. The images were obtained by a thermography device.

1.2 Thermal convection for a double pipe-type heat exchanger

The other type of thermal management, thermal convection, is studied in this experiment. Thermal convection is the heat transfer process for a fluidic medium and frequently utilized for efficient heat removal or heating of fluidic reactants in chemical plants. Different from the thermal conduction, which is usually studied in the general physics, thermal convection is often not well understood by undergraduates because rigorous calculations are needed for fluids based on the complicated partial differential equations based on the Naviers-Stokes equation under the requirement of the heat balance equation, and more profound knowledge is necessary to understand the whole theory. However, in chemical engineering, the thermal transport by fluids is treated by heat transfer coefficients, and the overall heat transfer coefficients are utilized as average heat transport. Different from the physical property values, the heat transfer coefficients are device-dependent, meaning the values depend on the device size, fluidic conditions, etc, and leaners understand that the values must be analyzed based on the non-dimensional numbers for different apparatus.

In thermal convection, a thermal boundary layer is assumed when the fluid is in contact with a solid surface. The heat transfer at the boundary is given by:

$$\mathrm{Q} = \frac{kA}{\delta}(T_1 - T_2), \tag{1.4}$$

where δ is the width of the boundary layer, k is the thermal conductivity, A is the area of thermal transport, and T_1 and T_2 are the high and low temperatures. δ cannot usually be calculated and is

(a)

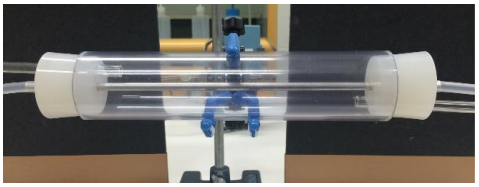

Double-pipe exchanger

(b)

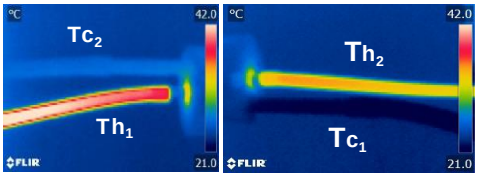

IR image taken by thermography

Fig. 3 (a) The apparatus of the double-pipe heat exchanger. A steel pipe was inserted inside a plastic tube. The heated air flew inside the steel pipe, while cold air flew inside the plastic pipe in the opposite direction. (b) The thermography images of the tubes connected to each end. T_{h1}, T_{h2}, T_{c1}, and T_{c2} correspond to the temperatures of the high-temperature fluids and the low-temperature fluids at the inlets and outlets, respectively.

dependent on fluidic conditions. The heat transfer coefficient is defined as follows:

$$h = \frac{k}{\delta} \tag{1.5}$$

In the case in which the two fluids are in contact with a thermally conductive layer, the overall heat transfer coefficient (U) is given as,

$$\frac{1}{UA} = \frac{1}{h_h A_h} + \frac{b}{\lambda A_{ave}} + \frac{1}{h_c A_c}, \tag{1.6}$$

where b is the thickness of the thermally conductive layer and where A_c and A_h are the contact areas for the cold and hot fluids. By using U, the overall heat transfer coefficient can be expressed as:

$$Q = UA\Delta T; \tag{1.7}$$

The thermal convection is understood based on the Nusselt number, one of the non-dimensional numbers, indicating the ratio of the contribution between the convective and conductive heat transports, and is given as,

$$Nu = \frac{hL}{\lambda}, \tag{1.8}$$

where L is the characteristic length of the thermal transport device. There are several empirical equations for the Nusselt number, depending on the device. For example, the Nusselt number is categorized separately for laminar and turbulent flows.

In this experiment, a double-pipe thermal exchanger was prepared, as shown in Figure 3. It is

frequently utilized for cooling fluidic reactants and products. The heat exchanger was built with a metal tube inside a plastic tube, and the heated air flew inside the metal tube while the cooled air was introduced into the plastic tube. By using a transparent plastic tube, the heat exchanging part was visible to learners. The temperatures at the entrances and exits for the low- and high-temperature fluids were directly monitored by thermography.

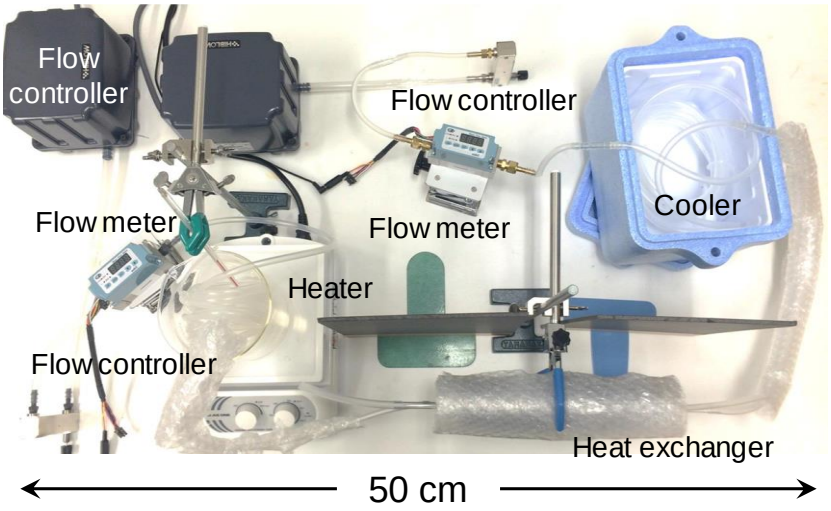

Fig. 4 The whole picture of the heat exchanger apparatus. The cool air was prepared by going through an iced water, and heated air was prepared by going through a heated water, and the air was pumped by two air pumps, and the flow rates was controlled by flow meters.

The overall equipment is shown in Figure 4. On one side, the air was heated by heating the tube inside a hot water bath. On the other side, it was cooled by cooling the tube inside a cooling bag. The fluid volume for each fluid was monitored by a flowmeter (Azbil, μFs). A hand-held thermography device (FLIR C2) was used to monitor the temperature for each tube. For different flow rates of the heated air, the net heat transfer coefficients were obtained. They were compared with the theoretical estimation using the Nusselt number (Figure 5). The agreement between the theory and the experiment was typically less than 10%.

The visibility of the thermal exchanger provides a good understanding of the mechanism. Additionally, the experiments using simple air help simplify the process. Soon after the fluids leave the exchanger, the learners can know the temperature, which fosters an intuitive understanding of the heat exchanger.

Flow volume / L・min^{-1}	$U_{experiment}$ / W・(m·K)$^{-1}$	$U_{calculation}$ / W・(m·K)$^{-1}$
14	31.8	29.4
12	30.8	28.0
10	29.5	26.3
8	23.4	24.2
6	15.4	16.3
4	14.1	14.9
2	10.3	12.6

※ Cool flow is constant at 8 L/min.

Fig. 5 The comparison between the overall thermal coefficients obtained from the experiment and theory. The flow rates of the heated air were varied, while that of the cool air was constant at 8 L/min.

2. Fluid engineering

2.1 Pressure drop in tubes and velocity measurements of fluids

Fluid control is necessary for the stable operation of chemical plants. Due to the friction between a tube wall and a fluid, additional pressure is needed to enable the flow of fluids, which is known as pressure drop. An educational experiment using microdevices was previously proposed (Groß *et al.*, 2010). To transport fluids, the dependence of the pressure drop on the size and structure of tubes, flow rate, and fluid viscosity must be understood. Furthermore, the fluidic profile is different from the laminar to turbulent type depending on the Reynolds number, which is defined by the force ratio between inertia and viscous force. This fluid-type transition is critically important for fluidic control. The pressure drop is described by the Fanning equation as:

$$\Delta P = 4f\left(\frac{L}{D}\right)\left(\frac{\rho U^2}{2}\right), \qquad (2.1)$$

where f is the frictional coefficient, L is the length, D is the diameter, ρ is the density, and U is the velocity. The dependence of pressure drop on the flow type – laminar or turbulent – is included in the friction coefficients, f, as:

$$f = \frac{16}{Re}, \qquad f = 0.079Re^{-\frac{1}{4}} \qquad (2.2)$$

for the laminar and turbulent flows, respectively, where Re is the Reynolds number, which defines

the transition from the laminar to the turbulent flow. Typically, the transition of the flow-type happens around 2300.

In this experiment, the pressure drop was measured by a silicone tube connected by plastic connectors to a digital manometer. The experimental setup is shown in Figure 6. After an adjustment of the pressure, air was pumped and sent into a silicone tube. The flow rate was measured by a flow meter (Azvil, μFs). When two T-type connectors are connected at the input and output of the tube, a pressure drop can be measured using a manometer (As One, DM-280) for a designated tube. Because various types of tubes and connectors can be inserted between the inlet and outlet of the air stream, learners can measure a pressure drop for the tubes and connectors. As an extended education, a pressure drop using a reducing connector, which is designed to connect tubes with different diameters, can be used for the calculation of the flow rate of the fluid. This is a simplified orifice meter for the flow rate measurements, which is a frequently used apparatus for fluid control.

An example of the dependence of pressure drop on the flow rate in a tube with an inner diameter of 3 mm is shown in Figure 7. The data clearly showed two regions of pressure drop, corresponding to the laminar and turbulent flows. Even for this simple device, learners can intuitively understand how the pressure drop is induced in a tube or a connecting part directly by replacing the parts, and also how the flow-type affects the pressure drop.

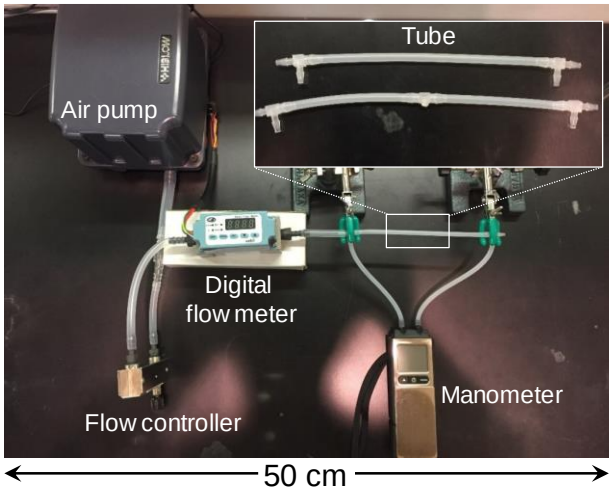

Fig. 6 The experimental apparatus of the pressure drop experiment. The air pump was used to flow air, while the flow rate was controlled by the flow controller and the air was sent into a tube. The pressure drop was measured between the measurement tubes, which had two outlet connectors. One of them was connected to a manometer. When a connector with a reducing diameter is utilized, it can be employed as a simplified orifice meter.

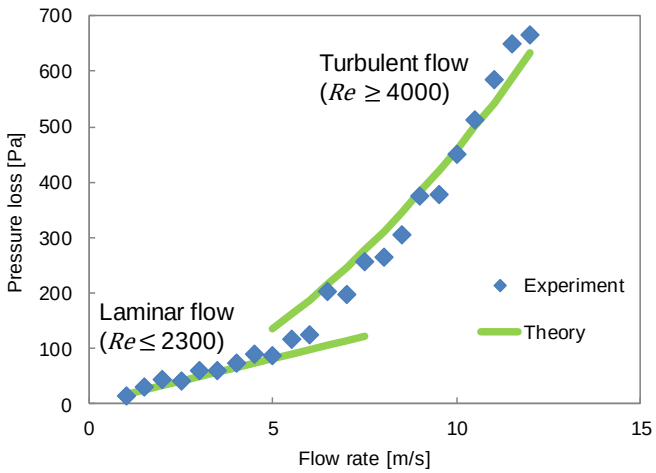

Fig. 7 The pressure loss curve vs flow rate is shown. The theoretically obtained fitting curves are also shown for the laminar and turbulent flow rate regions.

3. Unit operations

3.1 Distillation

There are many unit operations in the chemical processes such as separation, extraction, mixing, etc. The learners need to study the role and objective of each operation. Distillation is one of the most familiar unit operations, which is for the condensation of chemicals from a mixture solution. In the distillation, the learners need to understand the phase diagram for the gas/liquid equilibrium, and the phase diagram is utilized to obtain the concentration of the condensed chemicals. Small-scale gas/liquid equilibrium and distillation experiments were proposed previously in the 1990s (Flash, 1990; Schwartz, 1992).

In the distillation of a mixture solution of two components, and assuming that x_1, x_2, y_1, y_2 are the molar fraction in the gas and liquid phases, the molar fraction of component 1 in the gas phase is given by:

$$y_1 = \frac{P_1}{P} = \frac{x_1 P_1^0}{P}, \tag{3.1}$$

where P is the total pressure and P_1^0 is the saturated vapor pressure of component 1, and the molar fraction in the liquid phase is given as:

$$x_1 = \frac{P - P_2^0}{P_1^0 - P_2^0} \tag{3.2}$$

and the saturated vapor pressure of pure chemicals is given by the Antoine equation as:

$$\log P^0 = A - \frac{B}{T+C}, \quad (3.3)$$

where A, B, C are the constants for each chemical. From these equations, x and y are obtained for various temperatures, and the x-y plot can be prepared theoretically. Experimentally, a solution of x is distilled and the obtained molar fraction of the residual, condensed from the gas phase, can be obtained as y. The relation between x and y can be plotted. By using the x-y plot, learners can obtain the molar fraction in the gas if the molar fraction in the liquid is given and it is understood how the liquid is condensed during each process.

Chemical plants frequently use multi-step distillation. Multiple heated chambers are overlaid and a part of the solution is sent into the condensed region, while the rest of the solution is sent into the collection region in each chamber. A portion of the gas condensed from the final chamber is taken from the distillation equipment as a final product.

In this experiment, a water/ethanol mixture is used, and the x-y plot is prepared from the theory and experiment, as shown in Figure 8. The experimental apparatus is shown in Figure 9. The distillation glassware for microscale experiment (Kontes, 14/10 Microflex glassware kits) was used for distillation, similar to the previous experiments (Schwartz, 1992). The distillation flask was heated in an aluminum bath that had been heated by a heater, and the cooling water was circulated by a water pump (Cole Parmer, Masterflex L/S). When a metal sponge was put on top of the distillation flask, the distillation could be modified to perform a hypothetical multi-step distillation, too. The amount of ethanol inside the residual liquid was measured by the refractive index with a refractometer. The calibration curve was measured in advance.

An example of the result is shown in Figure 8. From the initial and final concentrations of ethanol,

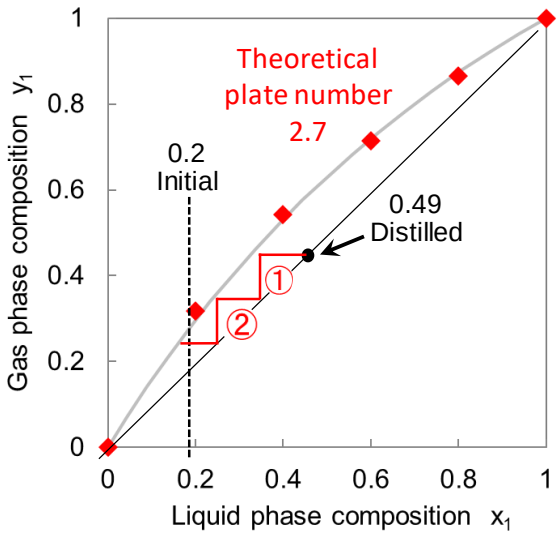

Fig. 8 Molar fraction in the liquid (x) and in the gas (y) are plotted to make a x-y plot. A calculation example for the multi-step distillation starting from x=0.2 is shown.

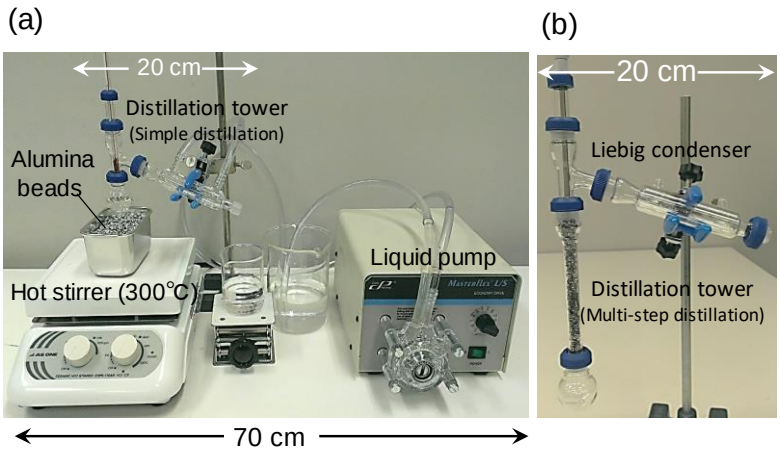

Fig. 9 The apparatus of small-scale distillation is shown. (a) The whole apparatus includes the heating bath and distillation glassware and the cooling water circulation. (b) The glassware of the small-scale distillation, and the distillation can be modified to perform a hypothetical multi-step distillation using aluminum foil.

the step-line was drawn to understand the plate number of the distillation. Unlike in the typical distillation experiment, the quantity of the used chemicals was almost 1/10, but still the principle and mechanism of the distillation can be sufficiently understood.

3.2 Adsorption of gas in solid medium

Adsorption is the process by which a specific species is condensed on a solid surface, such as deodorizing using activated carbon. This process is frequently utilized for the removal of unnecessary chemicals (Srisuda and Virote, 2008) or the collection of needed chemicals (Kirchstetter *et al.*, 2001). In this experiment, silica gel and water vapor were utilized as an adsorbent and an adsorbate, while a breakthrough curve was obtained to understand the performance of an adsorption column.

When gas is equilibrated with a solid adsorbent, the amount of adsorbate on the surface is expressed by an adsorption isotherm, such as the Langmuir equation. When a fluid including adsorbate is flown into the adsorption column, the adsorption equilibrium is reached from the entrance of the column. The adsorption itself happens in the finite region of the column, which is called an adsorption band. The band position gradually proceeds toward the direction of flow by saturating the adsorption on the solid surface from the entrance side. The adsorbate will gradually come out when the adsorption band is close to the end of the column. Assuming the initial concentration C_0 of the adsorbate, and the output concentration C_θ at time θ, the curve of C_θ/C_0 vs time is called the breakthrough curve. The length of the adsorption band can be calculated from the breakthrough curve, which is utilized for the breakthrough time of another adsorption column with a different length.

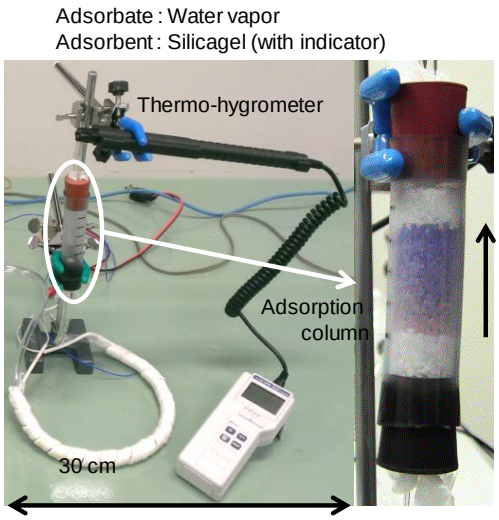

Fig. 10 The apparatus of vapor adsorption by an absorption column packed with silica gel particles is shown. Vapor with a humidity of 90% is sent from the bottom of the column, and the hygrometer is used to measure the humidity of the vapor at the exit.

In this experiment, an adsorption column is prepared by packing silica gel particles into a plastic tube as shown in Figure 10. Air with 90% humidity was sent into the adsorption column by an air pump, and a hygrometer was used to measure the humidity at the outlet (As One, TH-321). An example of the breakthrough curve is shown in Figure 11, along with the color change of the silica gel over time. The silica gel particles can be used repeatedly by heating up to remove the adsorbed water. This visual change will not only help create an understanding of the adsorption process but also provide information about the adsorption band and the breakthrough time.

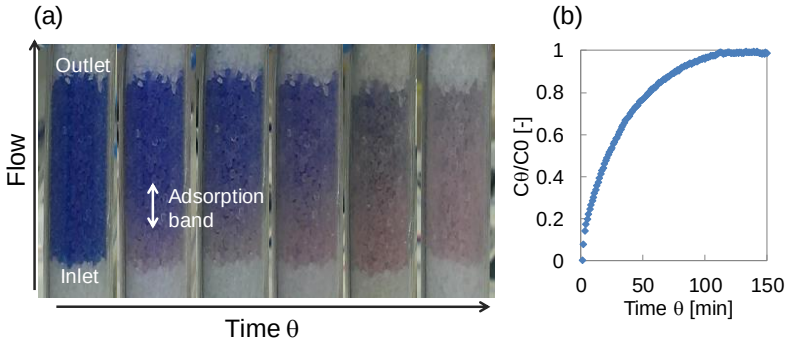

Fig. 11 (a) Pictures of the absorption column are shown in a series of time sequences. (b) A breakthrough curve obtained from the humidity measurement is shown.

3.3 Gas absorption

In chemical syntheses, harmful or unwanted gases are sometimes generated and therefore must be removed (Zidar *et al.*, 1997; Li *et al.*, 2017). In chemical plants, an absorption tower is utilized, where various types of sorbents are typically packed and water or other solvents (absorption liquid) is flown down from the top, while the gases are flown in the direction opposite from the bottom (Liu *et al.*, 2013). Through the contact of the gas and liquid at the solid/liquid interface, the unwanted gas is removed by solubilization into liquid.

In chemical engineering, the "double film" theory is introduced for the gas/liquid interface. Because it is difficult to obtain accurate concentrations and/or partial pressures at the real interface, the mass transfer coefficients in the gas and liquid are approximated. The mass flux of component A is expressed as:

$$N_{\mathrm{A}} = K_G(P - P^*) = K_L(C^* - C) = K_y(y - y^*) = K_x(x^* - x) \qquad (3.4)$$

where P* and C* are the pressure and concentration equilibrated with the concentration on the liquid side (C) and the pressure on the gas side (P), respectively, and where the corresponding molar fractions in the gas and liquid are y, y*, x, and x*, and the proportional coefficients – namely, the mass transfer coefficients – are regarded as K_G, K_L and Kx, Ky.

Assuming the counter-propagating gas absorption equipment as shown in Figure 12(a), the mass conservation gives the following equation:

$$G_{\mathrm{M}}\left(\frac{y_i}{1-y_i} - \frac{y_f}{1-y_f}\right) = L_{\mathrm{M}}\left(\frac{x_f}{1-x_f} - \frac{x_i}{1-x_i}\right) \qquad (3.5)$$

where G_M and L_M correspond to the molar flow rate of the target molecule in the gas and liquid sides, respectively.

The combination of the molar fractions at the top and bottom of the absorption equipment, (x_i, y_i) and (x_f, y_f), provides the operation line of the gas absorption, which is different from the equilibrium line of the gas and liquid, (x*, y*). This difference is the driving force for the gas absorption to the liquid phase. From the experiment, learners can measure the molar ratio at the entrance and exit of the gas absorption equipment and understand the flow rate dependence of the gas absorption.

For this purpose, we prepared an absorption tower packed with plastic balls, each of which had a diameter of 6 mm; they were toy bullets made of plastic (Figure 12). In real absorption equipment, packing materials such as a Raschig ring are utilized, but this simple absorption tower provided good visibility of the flow condition and absorption processes. Water flows from the topside by a liquid pump (As One, TP-20SA), while a mixture gas of carbon dioxide and air in a ratio of 1:3 flew from the bottom side. The absorption quantity of CO_2 into the water was measured by back titration. $Ba(OH)_2$ was added initially to precipitate CO_2 as $BaCO_3$; the remaining $Ba(OH)_2$ was titrated by HCl. When the concentration of CO_2 became constant (10 minutes), the molar ratio of CO_2 at the outlet was determined. In this experiment, the operation lines for different flow rates of the mixture gas were

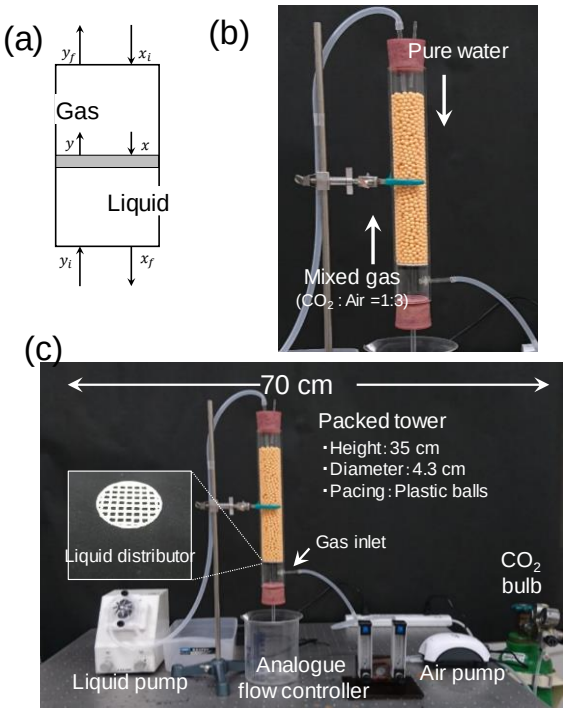

Fig. 12 (a) Schematic drawing of the gas absorption is shown. (b) The expanded picture of the absorption column is shown. (c) The whole apparatus includes the liquid pump and air pump; 20 vol% carbon dioxide gas is sent from the bottom side and water flow is sent from the top side.

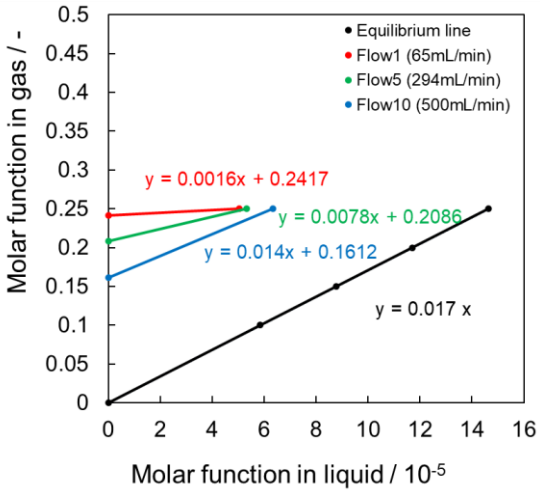

Fig. 13 The operation lines for the gas absorption are shown for different flow rates. The equilibrium line of carbon dioxide is also shown.

prepared and were plotted with the equilibrium line, as shown in Figure 13.

By using the visible absorption equipment and the quantitative determination of absorbed gas, learners could intuitively understand the absorption process and the dominant parameters to control the processes. This was possible because the experiment utilized safe gas and general commodity.

4. Reaction engineering

4.1 Reaction rate difference for various reactors

Unlike lab-scale synthesis, various types of reactors – especially continuous flow reactors – are frequently used for mass production in chemical plants. The reaction rate depends on the reactor type, size, and flow rates, and such parameters must be optimized for stable production (Taipa *et al.*, 2015) In this experiment, the two typical types of flow reactor models have been developed; learners can understand how the reactor type influences the reaction rate.

Flow reactors can be categorized into two typical types of reactors: the continuous stirred tank reactor (CSTR) and the piston flow reactor (PFR). Ideally, the concentrations of chemicals are assumed to be constant inside the tank for the CSTR, while they gradually change in terms of flow direction in the PFR. In both reactors, the mass balance is governed by the following equation:

$$F_{\mathrm{A0}} - F_{\mathrm{A}} + G_{\mathrm{A}} = \frac{dn_A}{dt}, \qquad (4.1)$$

where F_{A0} and F_A are the influx and the outflux of chemical A for the designated reactor region, G_A corresponds to the increase/decrease due to chemical reactions, and $\frac{dn_A}{dt}$ is the molar change rate of species A. The space-time, indicating the resident time of chemical species inside the reactor, is defined by

$$\tau_{\mathrm{m}} = \frac{V_m}{v_0}, \qquad (4.2)$$

where V_m corresponds to the volume of the reactor and v_0 is the flow volume rate of the reactant solution. In CSTR, the space-time is defined by

$$\tau_{\mathrm{c}} = \frac{C_{A0}x_A}{-r_A(x_A)} = \frac{C_{A0}}{-r_A(x_A)}(x_{\mathrm{A}} - 0), \qquad (4.3)$$

where C_{A0} and x_A are the initial concentration of the reactant and the molar fraction, respectively, and $(-r_A)$ corresponds to the reaction rate. For the first-order reaction, it is given by

$$k\tau_{\mathrm{c}} = \frac{x_A}{(1-x_A)}, \qquad (4.4)$$

In PFR, the space-time is defined by

$$\tau_{\mathrm{p}} = \frac{V_{\mathrm{p}}}{v_0} = C_{A0}\int_0^{x_{\mathrm{A}}} \frac{dx_A}{-r_A(x_A)}, \qquad (4.5)$$

and for the first-order reaction, it is given by

$$k\tau_{\mathrm{p}} = -ln(1 - x_{\mathrm{A}}), \qquad (4.6)$$

This experiment uses two hypothetical model reactors (CSTR and PFR), as shown in Figure 14.

The CSTR was prepared using a Teflon container connected to inlet and outlet tubes, while the PFR was prepared using a tube rolled around a pipe. The reactor volumes were set almost the same for both types of reactors. For the reaction, we selected the hydrolysis of ethyl acetate. Ethyl acetate and hydrochloric acid as a catalyst were pumped using a syringe pump (YMC, YSP-202) and the mixed solution was sent into the reactor (Figure 14). By changing the flow rate of the syringe pump, the space-time was controlled. For several different space-times, the reaction was performed and the acetic acid as a product was quantitated. A typical comparison for the reactions by the CSTR and PFR is shown in Figure 15. From this reaction rate dependence on the space-time, learners can calculate the reaction rate and understand the difference between the reactors.

This visual observation of reactions in two types of reactors can enhance the understanding of the reaction rate of chemical reactions, especially the difference between the two reactors.

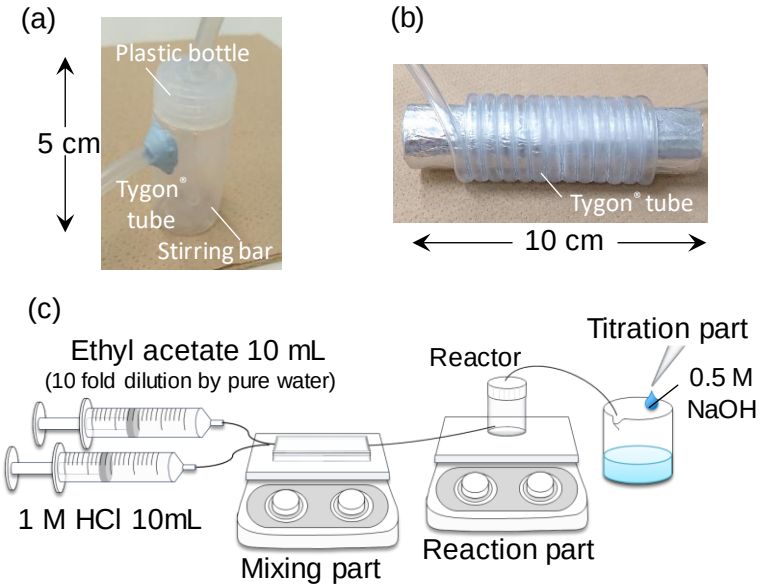

Fig. 14 Small-scale continuous reactors are shown: (a) continuous stirred flow reactor (CSTR) and (b) piston tube reactor (PFR). (c) The whole apparatus for the hydrolysis reaction of ethylacetate is shown. Two solutions were pumped by syringes, mixed, and sent to a reactor. The solution at the exit was titrated to calculate the acetate concentration.

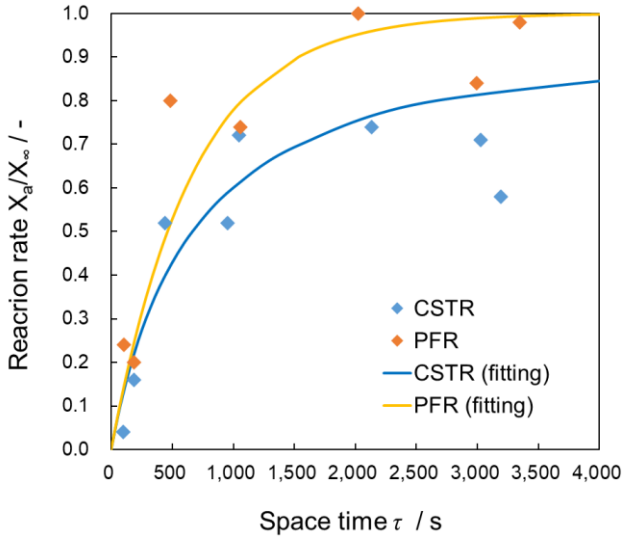

Fig. 15 The reaction rates for different reactors are shown with theoretical fitting curves for both the PFR and CSTR reactors.

4.2 High-pressure gas

For syntheses in chemical plants, high-pressure conditions are frequently necessary, such as for syntheses of ammonia and the polymerization of ethylene. It is important to understand the behavior of high-pressure gas to properly utilize reaction vessels and cylinders for high pressure. Under high-pressure conditions, an ideal gas equation of state cannot describe the gas behavior due to the non-negligible molecular interaction and size. Thus, various modifications have been made for the equation of states for real gas, such as the van der Waals equation. In this experiment, a compact high-pressure vessel was prepared and the pressure of the supercritical carbon dioxide was measured. Learners can understand the treatment and behavior of high-pressure gas.

The best-known modification for the equation of state was proposed in 1873 by van der Waals (Klein, 1974), is as follows:

$$P = \frac{\mathrm{R}T}{V_\mathrm{m} - b} - \frac{\mathrm{a}}{V_\mathrm{m}^2}, \tag{4.7}$$

where a and b are the adjustment parameters, including the effect of the molecular interactions. Further modifications have been made to the van der Waals equation. This experiment utilized two typical ones: the SRK (Soave-Redlich-Kwong) and PR (Peng-Robinson) equations, as follows:

$$P = \frac{\mathrm{R}T}{V_\mathrm{m} - b\prime} - \frac{\alpha\prime(T)}{V_\mathrm{m}(V_\mathrm{m} + b\prime)}, \tag{4.8}$$

$$P = \frac{RT}{V_m - b''} - \frac{\alpha''(T)}{V_m(V_m + b'') + b''(V_m - b'')}, \quad (4.9)$$

The difference between the van der Waals equation and these equations is that the latter have temperature-dependent parameters to adjust them.

In this experiment, a compact high-pressure vessel (316L-50DF4-150, Swagelok) equipped with a pressure gauge, as shown in Figure 16, was prepared to create the supercritical condition of CO_2. After CO_2 was injected into the vessel, the increase in weight was measured using a scale. The vessel was then put into a thermostatic bath set at 40°C. After the equilibrium condition was reached, the gauge was used to measure the pressure. After the release of some gas (controlled by the release time), the weight of the vessel was measured again and the pressure was read. This process was repeated to create the pressure-molar volume curve, as shown in Figure 17. The difference from the theoretical curve from the ideal gas is clearly understood. However, the difference between the equations of state for real gas cannot be compared due to the accuracy of the pressure gauge. but it is also a good way to understand how accurate the measurement is.

Learners can understand the difference in behavior of the high-pressure gas and can also gain experience in the preparation of the high-pressure gas. Due to the accuracy of the pressure gauge, the difference between the theories could not be compared in this experiment; however, learners can understand it by using theoretical calculations.

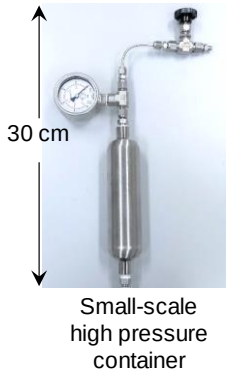

Fig. 16 A small-scale, high-pressure container with a pressure gauge and a bulb.

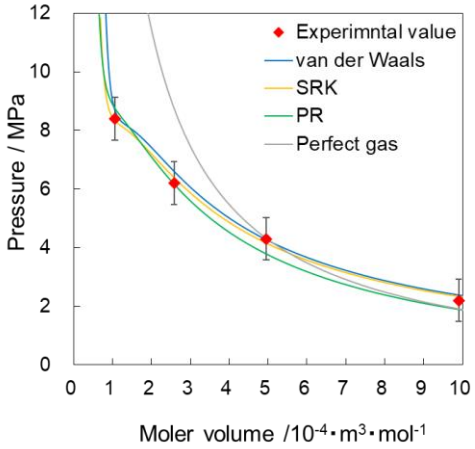

Fig. 17 P-V_m curve obtained from the high-pressure experiment of CO_2. Theoretical curves obtained for the perfect gas and for the real gas from other theoretical equations are shown together.

5. Others

5.1 Particle size measurement

In the chemical industry, granulation is an important process for preparing medicine and fine chemicals as well as for controlling food qualities, such as smoothness and taste. Furthermore, particle synthesis is frequently used in the polymer industry; the size and homogeneity control of the particles is important for stable production (Morgan and Kaler, 1998). Various methods have been utilized to control the particle size and distribution. In this experiment, the microscopic method and the screening method are selected to obtain an intuitive understanding of particle size and distribution.

Usually, the particle size distribution is understood using the histogram for the size of particles. The residual weight (number) ratio, R, which means the weight (number) ratio for the particles with their diameter > d, is plotted, and the mode diameter is obtained at the diameter where R is equal to 0.5.

In this experiment, two experiments were prepared using a compact shaking apparatus (As One, MVS-1N) with a height of 30 cm for millimeter-scale stones and a USB microscope (Sanwa Supply 400-CAM058) with a height of 15 cm for micrometer-scale particles, as shown in Figure 18. In the shaking apparatus, screen media with different mesh sizes were over-layered and gravel was separated in terms of size. In the microscopic method, a mixture of glass beads with a diameter range from 3 to 20 μm was observed, while the size distribution was directly analyzed by ImageJ (Schneider *et al.*, 2012). The procedures for the experiments are summarized by the schemes in Figure 19. One of the results of the microscopy method is shown in Figure 20. The size distribution of particles was obtained from the graph display of the histogram and the R curve.

From this experiment, learners can intuitively understand the size distribution from the microscopic image and the separated ravels, as well as understand the histogram method and the R

curve.

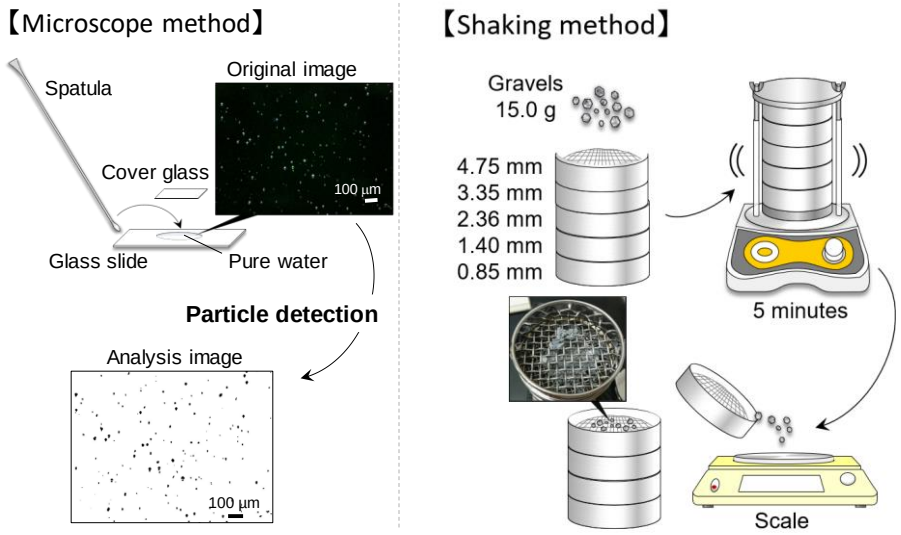

Fig. 18 The procedures for measuring particle size for the microscopic method and the shaking method are summarized in the schemes.

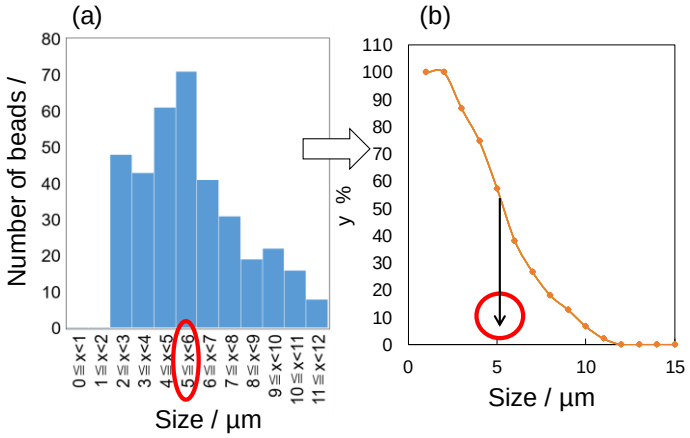

Fig. 19 (a) The size distribution histogram for the data obtained by the microscopic measurement. (b) The corresponding R curve and how to obtain the mode diameter.

Conclusion

The series of experiments intended to educate undergraduate students in a chemical engineering course are summarized. In developing the experimental series, we extended the concept of the "small-scale/micro-scale experiment" and emphasized the intuitive understanding of various processes in chemical engineering, which have frequently been "black box." Students can see a compact-size

experiment carried out directly in front of them, and the visibility of the experiment helps the students develop an intuitive understanding of the phenomenon in question. All the courses have already been utilized in chemical engineering education at our university. This series could not cover all the subjects, but continued efforts to develop new experiments focusing on a similar concept would cover the entire range of subjects in the near future.

Acknowledgments

The research was financially supported by Chuo University, JST (#11102170, # 12101862).

Conflicts of Interests

There are no conflicts to declare.

References

Brooks H. B. and Brooks D. W., (1995), Small Scale Electrophoresis. *J. Chem. Educ.*, **72**(2), A28–A29.

Brouwer H., (1991), Small-scale thermochemistry experiment. *J. Chem. Educ.*, **68**(7), A178–A181.

Chien S.-I., Su C., Chou C.-C., and Li W.-R., (2018), Visual Observation and Practical Application of Dye Sensitized Solar Cells in High School Energy Education. *J. Chem. Educ.*, **95**(7), 1167–1172.

El Seoud O. A., Loffredo C., Galgano P. D., Sato B. M., and Reichardt C., (2011), Have Biofuel, Will Travel: A Colorful Experiment and a Different Approach To Teach the Undergraduate Laboratory. *J. Chem. Educ.*, **88**(9), 1293–1297.

Feng Z. V., Edelman K. R., and Swanson B. P., (2015), Student-Fabricated Microfluidic Devices as Flow Reactors for Organic and Inorganic Synthesis. *J. Chem. Educ.*, **92**(4), 723–727.

Flash P., (1990), A small scale equilibrium experiment. *J. Chem. Educ.*, **67**(4), 341.

Gilow H. M., (1991), Free radical halogenation of hydrocarbons: Experiments for organic chemistry using the small-scale approach. *J. Chem. Educ.*, **68**(5), A122–A124.

Grønneberg T., Kvittingen L., and Eggen P.-O., (2006), Small-Scale and Low-Cost Galvanic Cells. *J. Chem. Educ.*, **83**(8), 1201–1203.

Groß A., Schneider S., Abahmane L., and Köhler J. M., (2010), Pressure Loss – Educational Experiments for Microreaction Technology using an Universal Experiment Platform. *Chem. Ing. Tech.*, **82**(10), 1789–1798.

Haglund J., Jeppsson F., Hedberg D., and Schönborn K. J., (2015), Thermal cameras in school laboratory activities. *Phys. Educ.*, **50**(4), 424–430.

Hatzikraniotis E., Kallery M., Molohidis A., and Psillos D., (2010), Students' design of experiments: an inquiry module on the conduction of heat. *Phys. Educ.*, **45**(4), 335–344.

Horak V. and Crist D. R., (1975), Small scale organic techniques: Filtration and crystallization. *J. Chem. Educ.*, **52**(10), 664–665.

Johnson S. M., Javner C., and Hackel B. J., (2017), Development and Implementation of a Protein–Protein Binding Experiment To Teach Intermolecular Interactions in High School or Undergraduate Classrooms. *J. Chem. Educ.*, **94**(3), 367–374.

Kelkar S. L. and Dhavale D. D., (2000), Microscale experiments in chemistry —The need of the new millennium. *Resonance*, **5**(10), 24–31.

Kirchstetter T. W., Corrigan C. E., and Novakov T., (2001), Laboratory and field investigation of the adsorption of gaseous organic compounds onto quartz filters. *Atmos. Environ.*, **35**(9), 1663–1671.

Klein M. J., (1974), The historical origins of the Van der Waals equation. *Physica*, **73**(1), 28–47.

Lee S. and Wiener J., (2011), Visualizing Chemical Phenomena in Microdroplets. *J. Chem. Educ.*, **88**(2), 151–157.

Li J., Zhou X., Zhang L., Di H., Wu H., and Yang L., (2017), Investigation on the Immobilization of Carbonic Anhydrase and the Catalytic Absorption of Carbon Dioxide. *Energy Fuels*, **31**(1), 778–784.

Liu Kun, Jinka K. M., Remias J. E., and Liu Kunlei, (2013), Absorption of Carbon Dioxide in Aqueous Morpholine Solutions. *Ind. Eng. Chem. Res.*, **52**(45), 15932–15938.

McKenzie L. C., Thompson J. E., Sullivan R., and Hutchison J. E., (2004), Green chemical processing in the teaching laboratory: a convenient liquid CO2 extraction of natural products. *Green Chem.*, **6**(8), 355–358.

Möllmann K.-P. and Vollmer M., (2007), Infrared thermal imaging as a tool in university physics education. *Eur. J. Phys.*, **28**(3), S37.

Morgan J. D. and Kaler E. W., (1998), Particle Size and Monomer Partitioning in Microemulsion Polymerization. 1. Calculation of the Particle Size Distribution. *Macromolecules*, **31**(10), 3197–3202.

Néel B., Cardoso C., Perret D., and Bakker E., (2015), A Miniature Wastewater Cleaning Plant to Demonstrate Primary Treatment in the Classroom. *J. Chem. Educ.*, **92**(11), 1889–1891.

Pavia D. L., Lampman G. M., Kriz G. S., and Engel R. G., (2007), *Introduction to Organic Laboratory Techniques A Microscale Approach*, 4th edition. Thomson Brooks/Cole.

Schneider C. A., Rasband W. S., and Eliceiri K. W., (2012), NIH Image to ImageJ: 25 years of image analysis. *Nat. Methods*, **9**(7), 671–675.

Schwartz M. H., (1992), Microscale distillation—Calculations and comparisons. *J. Chem. Educ.*, **69**(4), A127–A128.

Selmer A., Kraft M., Moros R., and Colton C. K., (2007), Weblabs in Chemical Engineering Education. *Educ. Chem. Eng.*, **2**(1), 38–45.

Skinner J., (1997), *Microscale Chemistry*, The Royal Society of Chemistry.

Sobral A. J. F. N., (2005), Synthesis of Meso-Octamethylporphyrinogen: An Undergraduate Laboratory Mini-Scale Experiment in Organic Heterocyclic Chemistry. *J. Chem. Educ.*, **82**(4), 618–620.

Squires R. G., Andersen P. K., Reklaitis G. V., Jayakumar S., and Carmichael D. S., (1992), Multimedia-based educational applications of computer simulations of chemical engineering processes. *Comput. Appl. Eng. Educ.*, **1**(1), 25–32.

Srisuda S. and Virote B., (2008), Adsorption of formaldehyde vapor by amine-functionalized mesoporous silica materials. *J. Environ. Sci.*, **20**(3), 379–384.

Stock J. T., (1990), Small-scale organic chemistry in retrospect. *J. Chem. Educ.*, **67**(10), 898–899.

Stock J. T., (1953), Small-scale techniques in the teaching of organic chemistry. *J. Chem. Educ.*, **30**(6),

296–304.
Supasorn S., (2015), Grade 12 students' conceptual understanding and mental models of galvanic cells before and after learning by using small-scale experiments in conjunction with a model kit. *Chem. Educ. Res. Pract.*, **16**(2), 393–407.
Szafran Z., Pick R. M., and Foster J. C., (1993), *Microscale General Chemistry Laboratory*, John Wiley & Sons, Inc.
Szafran Z., Pike R. M., and Singh M. M., (1991), *Microscale Inorganic Chemistry*, John Wiley & Sons, Inc.
Tabassum T., Iloska M., Scuereb D., Taira N., Jin C., Zaitsev V., et al., (2018), Development and Application of 3D Printed Mesoreactors in Chemical Engineering Education. *J. Chem. Educ.*, **95**(5), 783–790.
Taipa M. Â., Azevedo A. M., Grilo A. L., Couto P. T., Ferreira F. A. G., Fortuna A. R. M., et al., (2015), Student Collaboration in a Series of Integrated Experiments To Study Enzyme Reactor Modeling with Immobilized Cell-Based Invertase. *J. Chem. Educ.*, **92**(7), 1238–1243.
Vrtacnik M. and Gros N., (2005), A Small-Scale Low-Cost Gas Chromatograph. *J. Chem. Educ.*, **82**(2), 291–293.
Wietsma J. J., van der Veen J. T., Buesink W., van den Berg A., and Odijk M., (2018), Lab-on-a-Chip: Frontier Science in the Classroom. *J. Chem. Educ.*, **95**(2), 267–275.
Wright G. F. and Eastcott E. V., (1949), Small-scale experiments for the organic chemical laboratory (Oxidation of para-nitrotoluene). *J. Chem. Educ.*, **26**(8), 406–408.
Zidar M., Golob J., Veber M., and Vlachy V., (1997), Absorption of SO2 into Aqueous Solutions. 2. Gas−Liquid Equilibrium of the MgO−SO2−H2O System and Graphical Presentation of Operation Lines in an Equilibrium Diagram. *Ind. Eng. Chem. Res.*, **36**(10), 4342–4346.
Zipp A. P., (1989), Introduction to "The Microscale Laboratory." *J. Chem. Educ.*, **66**(11), 956–957.